MethodsX 11 (2023) 102445

Contents lists available at ScienceDirect

MethodsX

journal homepage: www.elsevier.com/locate/methodsx

# Experimental procedures to investigate fibrillation of proteins

Chinmaya Panda, Laipubam Gayatri Sharma, Lalit M. Pandey*

*Bio-interface & Environmental Engineering Lab, Department of Biosciences and Bioengineering, Indian Institute of Technology Guwahati, Assam 781039, India*

ARTICLE INFO

*Method name:*
Study of protein unfolding and aggregation

*Keywords:*
Amyloid
Circular dichroism
Atomic force microscopy
Fibrillation
Bovine serum albumin

ABSTRACT

The unwanted phenomenon of protein fibrillation is observed *in vivo* and during therapeutic protein development in the industry. Protein aggregation is associated with various degenerative disorders and might induce immune-related challenges post-administration of biopharmaceutics. A pipeline for early detection, identification, and removal of pre-formed fibrils is needed to improve the quality, efficacy, and effectiveness of the formulation. Protein fibril formation is accompanied by unfolding, secondary structural changes and the formation of larger aggregates. However, most detection processes come with extensive sample preparation steps and inefficient repeatability, incurring a financial burden on research. The current article summarizes and critically discusses six simple yet powerful methods to detect aggregation phenomena in the line of detecting fibrillar aggregates in heat-induced bovine serum albumin protein. Comparing the native and heat-induced protein samples would provide insights about aggregates. Easy, inexpensive and optimized protocols for detecting the fibrillation of proteins are explained. The procedures mentioned here detected the appearance of $\beta$-sheet-rich fibrils in the heat-induced protein sample. The aggregation is characterized by enhanced thioflavin-T fluorescence, alteration in the intrinsic fluorescence, decrease in helicity and subsequent increase in $\beta$-sheet and appearance of particles with larger hydrodynamic diameters.

- This article summarizes various analytical techniques to easily characterize the fibrillation of proteins.
- Various techniques to detect the formation of $\beta$-sheet rich structures, changes in the secondary structures and size of aggregates have been discussed.
- The stated methodologies are validated on a model protein, albumin.

## Specifications table

| | |
|---|---|
| Subject area: | Biochemistry, Genetics and Molecular Biology |
| More specific subject area: | Biotechnology and Bioengineering |
| Name of your method: | Study of protein unfolding and aggregation |
| Name and reference of original method: | NA |
| Resource availability: | Please refer to Table 1 |

* Corresponding author.
*E-mail address:* lalitpandey@iitg.ac.in (L.M. Pandey).

https://doi.org/10.1016/j.mex.2023.102445
Received 2 January 2023; Accepted 16 October 2023
Available online 17 October 2023

## Introduction

The aggregation of proteins is pervasive not only within a biological perspective but also in biotherapeutics development. Under unfavorable conditions encompassing multiple biological, physicochemical, and environmental factors, proteins tend to lose their native structure, forming unfolded and partially misfolded intermediates [1]. These factors operate at a cellular and biopharmaceutical product development level, ranging from cellular mutations, aging, oxidative stress, and dysfunctional chaperones to temperature, pH, shear, and air-water interface [2]. Considering the notion of protein folding funnel, misfolded protein intermediates are deemed to be thermodynamically unstable and thus form higher-ordered disordered aggregates. Intermolecular interactions prevail during this off-pathway of protein folding, finally forming stable amyloid fibrils via electrostatic, Van der Waals, H-bonding, and aromatic stacking interactions [2].

In the case of pharmaceutical product development, protein fibrillation has been linked with decreased formulation stability and reduced efficacy, ultimately posing a threat to patient health, and triggering an immune response [3]. In an *in vivo* cellular setting, however, protein unfolding and subsequent fibrillation have been linked with protein misfolding-related inflammation and degenerative disorders, such as Alzheimer's disease, Parkinson's disease, Creutzfeldt-Jakob disease, Huntington's disease, cystic fibrosis, and other neurodegenerative disorders [4]. The demand for effective therapeutics and efficient risk assessment approaches have necessitated improved *in vitro* and *in vivo* amyloid fibril detection methods. As amyloids contain a high percentage of $\beta$-sheet conformations, biophysical, analytical, and microscopic methods that faithfully detect protein secondary structure are rendered beneficial.

Though there exist multiple studies using advanced and diverse methods to detect protein fibrillation, there is an utmost need to summarize and verify the methods for protein fibrillation detection using easily accessible and available lab resources, rather than using complicated techniques. In this method article, an attempt has been made to study the fibrillation of a model protein, bovine serum albumin (BSA). This study validates the key techniques used for such investigations like direct or indirect secondary structure determination methods using circular dichroism (CD) spectroscopy, Fourier-transform infrared (FTIR) spectroscopy, intrinsic fluorescence spectroscopy and thioflavin-T (ThT)-binding assay. The morphological analysis has been performed using dynamic light scattering (DLS) and atomic force microscopy (AFM). Two different samples of the protein are considered, one being the native BSA, while the other being BSA heated at 60 ˚C for overnight. This aforementioned methods may also be used for detecting the aggregates of other proteins or peptides, such as insulin, A$\beta$ peptide and tau peptide [5,6].

## Material and reagents

Table 1 summarises the overall methodologies and resource requirements. Individual methods are discussed as follows:

### *Tris buffer saline (TBS) buffer*

- Dissolve 1.97 gm (25 mM) of Tris–HCl (Himedia, Mumbai, MH, India, Cat: TC073), 3.65 gm (125 mM) NaCl (Himedia, Mumbai, MH, India, Cat: GRM853), and 0.095 gm (2 mM) of $MgCl_2$ (Himedia, Mumbai, MH, India, Cat: MB237) in 450 ml of MilliQ water.
- Adjust the pH to 7.4, followed by making up the volume to 500 ml.
- Filter the TBS buffer solution with a 0.22 µm polyethersulfone (PES) filter (Axiva Sichem Biotech, Delhi, India, Cat: SFPS25R). Store the buffer at 4 ºC for further use.

### *Thioflavin-T (ThT) assay*

ThT has been widely used as an indicator dye for detecting amyloid fibrillation *in vitro* [5,7]. This dye bind to amyloid fibrils with $\beta$-sheet rich structures and, provides a fluorescence signal at around 482 nm upon excitation at 450 nm [8]. Though the exact mechanism of ThT fluorescence enhancement upon binding to amyloid fibrils is debatable, but the rotational immobilization of the connecting carbon-carbon bond between benzothiazole and aniline rings is attributed to the same [9]. ThT is supposed to bind to the long amyloid fibril axis along with the consecutive $\beta$-strands [9]. To evaluate the temperature-induced bovine serum albumin (BSA) protein fibrillation, the following methods have been followed:

- Prepare a stock solution of bovine serum albumin (BSA) (Sigma-Aldrich, Darmstadt, Germany, Cat: A2153) in TBS buffer and filter it through the 0.22 µm PES filter.
- Dissolve 3.18 mg of ThT (Sigma-Aldrich, Darmstadt, Germany, Cat: T3516) in 10 ml of TBS buffer to prepare the stock solution. Filter the solution through a 0.2 µm PES syringe filter.
- For setting up the fibrillation process, keep 1 ml of the BSA working solution in an incubator at 60 ˚C for overnight.
- The ThT assay is to be performed in a Corning® dark flat-bottom plate (Corning, NY, USA, Cat: CLS3603). Dilute ThT with TBS buffer, so the final working ThT concentration in the well will be 20 µM.
- Maintain BSA concentration in the well as 1:2 of BSA to ThT.
- Seal and place the plate in an incubator at 37 ˚C for 10 min.
- ThT is known to specifically bind to amyloid fibrils with an excitation/emission wavelength of 450/482 nm. So, perform fluorescence measurements on a Tecan Infinite 200 pro (Tecan, Zurich, Switzerland) multimode microplate reader with 5 nm of excitation and emission slits.

**Table 1**
List of the overall methodologies used to investigate the fibrillation of proteins and resource requirements.

| Process | Reagent, equipment, and software | Time and economic requirements |
|---|---|---|
| Thioflavin-T binding assay | 1. Bovine serum albumin (BSA) (Sigma-Aldrich, Darmstadt, Germany, Cat: A2153)<br>2. 0.22 μm polyethersulfone (PES) filter (Axiva Sichem Biotech, Delhi, India, Cat: SFPS25R)<br>3. Thioflavin-T (ThT) (Sigma-Aldrich, Darmstadt, Germany, Cat: T3516)<br>4. Corning® dark flat-bottom plate (Corning, NY, USA, Cat: CLS3603)<br>5. Incubator maintaining temperature up to 60 °C<br>6. Tecan Infinite 200 pro (Tecan, Zurich, Switzerland) multimode microplate reader | • It is a destructive method and samples cannot be recovered or reused.<br>• Requirements of dark flat-bottom plates and a multimode microplate reader may make the process a little bit expensive.<br>• Consumes less time. |
| Circular dichroism (CD) spectroscopy | Apart from the usual requirements of BSA, buffer, and PES filters, the following components are required:<br>1. JASCO J-1500 CD spectrophotometer (JASCO, Tokyo, Japan)<br>2. Nitrogen cylinder<br>3. CD-specific cuvette<br>4. Spectra Manager™ (JASCO, Tokyo, Japan)<br>5. DichroWeb (accessible at: http://dichroweb.cryst.bbk.ac.uk/) | • CD spectroscopy is usually a non-destructive method and requires very less volume of sample.<br>• The instrument is extremely sensitive, however requires nitrogen purging. Therefore, an additional nitrogen generator is required, making the complete process expensive. |
| Fourier-transform infrared (FTIR) spectroscopy | Apart from the usual requirements of BSA, buffer, and PES filters, the following components are required:<br>1. Spectrum Two spectrophotometer (PerkinElmer, Waltham, MA, USA)<br>2. Spectrum™ software (PerkinElmer, Waltham, MA, USA)<br>3. OMNIC™ Specta Software (Thermo Fisher Scientific, Waltham, MA, USA)<br>4. Bry-air dehumidifier | • FTIR, even though is a non-destructive method, but requires a relatively higher concentration of sample.<br>• It further requires $D_2O$, and a nitrogen-purged environment to avoid interference from the O–H bond. |
| Dynamic light scattering (DLS) | Apart from the usual requirements of BSA, buffer, and PES filters, the following components are required:<br>1. Litesizer 500 (Anton Paar, Graz, Austria)<br>2. DLS-specific cuvette | • DLS is a relatively cost-effective and easy-to-use equipment without the requirement of additional analytical software.<br>• However, only the overall particle size is generated, without much information about particle morphology. |
| Intrinsic Fluorescence | 1. FluoroMax-4 fluorimeter (Horiba Scientific, Kyoto, Japan).<br>2. Fluorometer specific 10 mm path length, four-sided transparent quartz cuvette | • FluoroMax is a non-destructive, cost-effective, and fast method to detect fluorescence spectroscopy.<br>• Through it requires a low concentration of protein; but needs relatively more volume of sample. |
| Atomic force microscopy (AFM) | 1. Cypher S AFM microscope (Oxford Instruments, High Wycombe, UK)<br>2. Carbon tapes, forceps, and scissors<br>3. Gwyddion software (accessible at: http://gwyddion.net/) | • AFM is a relatively expensive method due to sophisticated instrumention.<br>• It is required to detect the morphology of protein aggregates.<br>• The sample preparation takes relatively more time. |
| Additional Requirements | 1. Tris–HCl (Himedia, Mumbai, MH, India, Cat: TC073),<br>2. Sodium chloride (NaCl) (Himedia, Mumbai, MH, India, Cat: GRM853)<br>3. Magnesium chloride ($MgCl_2$) (Himedia, Mumbai, MH, India, Cat: MB237)<br>4. MilliQ® Ultrapure Water Systems (Merck Millipore, Darmstadt, Germany) | |

- All the procedures for the ThT experiment are to be performed in the dark to avoid fluorescence decay.
- Repeat the experiment at least three times, keeping all parameters constant across the replicates.
- Plot a ThT fluorescence graph along with the standard deviation for both native and heat-induced BSA.

*Intrinsic fluorescence spectroscopy*

Absorbance spectroscopy can also be used to monitor the conformational transitions in proteins. Owing to the natural absorption phenomena, tryptophan residues are generally used for monitoring the structural changes in a protein [10]. Tryptophan is the

most important chromophore in the UV region of a protein. On the other hand, tyrosine and phenylalanine contribute to intrinsic fluorescence in a lesser proportion [11]. Owing to the indole ring of tryptophan and the phenol ring of tyrosine, these residues become sensitive to solvent polarity, which in turn can be used for detecting the unfolding and aggregation of protein by monitoring absorbance [12]. The intrinsic fluorescence of the native and the heat-induced BSA samples is determined using the FluoroMax-4 fluorimeter (Horiba Scientific, Kyoto, Japan).

- Dilute the native and heat-induced protein samples to a final working concentration of 2 μM (the ideal absorbance should be ~ 0.05 AU).
- Pipet 1 ml of sample in a 10 mm path length, four-sided transparent quartz cuvette.
- Set the excitation wavelength at 280 nm and record the emission spectrum from 300 to 450 nm.
- Keep the bandwidth of the excitation and the emission as 5 nm and 10 nm, respectively, with a total of 5 run accumulations per a given sample to obtain a final average spectrum.
- Perform the experiment for native and heat-induced samples keeping all other parameters constant.
- Subtract the buffer spectrum from both the native and heat-induced BSA spectra with the baseline correction function.
- Plot a graph of the absorbance (in AU) across the wavelength for both native and heat-induced BSA.

*Circular dichroism (CD) spectroscopy*

A CD spectrum in the far ultraviolet (UV) region determines peptide bond orientations and the bond energy level transitions. In a native protein structure, peptide bonds are arranged in an orderly manner at a stable energy state [13]. However, due to perturbed physicochemical and structural parameters, variations in the bonding pattern occur in a disordered protein, leading to changes in the CD spectrum [14]. For secondary structure analysis and further detection of conformational changes of BSA protein samples, far-UV CD spectroscopic measurement is performed in a JASCO J-1500 CD spectrophotometer (JASCO, Tokyo, Japan) over the wavelength range of 190–260 nm [15,16]. The following protocol is employed:

- Turn on $N_2$ gas and maintain a constant flow rate of 5 liters/min.
- Wait 20 min to purge the system entirely with $N_2$ gas.
- Dilute and filter the BSA protein solution to a working concentration of 0.2 mg/ml.
- Pipet 300 μl of TBS buffer in a CD specific rectangular quartz cuvette of 0.1 cm of path length.
- Ensure considering the buffer as a baseline and then pipet 300 μl of native protein sample solution.
- Measure the CD (mdeg). The HT voltage should be less than 650 V, and the number of accumulations is limited to 10 with a scanning speed of 50 nm/minute.
- The data pitch remains 0.1 nm with a bandwidth of 1 nm.
- The following equation is used in the DichroWeb online webserver for converting the CD signal output ($\theta$) in millidegree (mdeg) to mean residue ellipticity value (MRE) in (deg $cm^2$ $dmol^{-1}$ $residue^{-1}$) [17].

$$\mathrm{MRE} = \theta \times \frac{(0.1 \times \mathrm{MRW})}{(\mathrm{P} \times \mathrm{C})} \tag{1}$$

where, MRW = mean residue weight of BSA = $\frac{\text{Molecular weight of BSA in daltons}}{\text{Number of residues}} = \frac{66400}{583} = 113.89$

$P$ = path length (in cm) = 0.1 cm

C = concentration of BSA (in mg/ml) = 0.2 mg/ml

- The above method is to be repeated for the heat-induced BSA sample as well.
- A graph is plotted for MRE against the wavelength values from 190 to 260 nm for both the BSA samples.
- The percentage of $\alpha$-helix, $\beta$-sheet, turn, and unordered conformations can be obtained with the help of online webservers such as DichroWeb [17], K2D3 [18], and BeStSel [19].

*Fourier-transform infrared (FTIR) spectroscopy*

FTIR spectroscopy is widely used as a non-invasive, non-destructive, and label-free method to detect the vibrational and rotational effects of the electromagnetic spectrum on peptide bonds [20]. As protein fibrillation is accompanied by three-dimensional changes in peptide bond orientations, an FTIR spectra in the Amide I (1600–1700 $cm^{-1}$) region primarily provides important structural information about the C=O stretching, and N-H bending variations across the backbone [21]. Therefore, a comparison-based study across the native and heat-induced samples would provide key structural features of the $\alpha$-helix, $\beta$-sheet, turn, and unordered conformations [20]. For the BSA solution, FTIR spectroscopy is performed using the Spectrum Two spectrophotometer (PerkinElmer, Waltham, MA, USA) based on the following methods:

- Prepare 20 mg/ml of BSA sample in deuterated water ($D_2O$).
- Due to the sensitivity of the $D_2O$ to the outer environment, make sure to add BSA inside a nitrogen-purged environment.
- Drop cast a sample volume of 20 μl of $D_2O$ on the diamond crystal in the attenuated total reflectance (ATR) mode for background scan. Set the number of scans to 10, at a resolution of 4 $cm^{-1}$, with the entire coverage spectra of 400–4000 $cm^{-1}$. Measure the spectra for the native and heat-induced BSA samples.
- Subtract the background spectrum from both the native and heat-induced BSA spectra with the baseline correction function.

- Resolve and de-convolute the recorded spectra with Gaussian curves using Origin 8.5 software (OriginLab Corporation, Northampton, MA, USA) to calculate the percentage secondary structure.

*Atomic force microscopy (AFM)*

Apart from the molecular spectroscopic characterization, microscopic observation of the native and heat-induced BSA solution also provides insights into protein fibrillation morphology [15,22]. Atomic force microscopy (AFM) is conducted using the Cypher S (Oxford Instruments, High Wycombe, UK) AFM microscope equipped with a silicon nitride tip in non-contact mode.

- Silicon wafer chips cut in about 0.5 × 0.5 cm is to be used as substrates.
- Wash the silicon wafer plates in acetone in a bath sonicator for about 15 min.
- The same process is repeated in MilliQ water and then the substrates are dried using lint-free tissue paper.
- Pipet and drop cast about 10 µl of 2 mg/ml protein solution on the dried and cleaned silicon wafer surface and let the solution adsorb for about 30 min.
- Carefully spray a thin stream of MilliQ water over the drop-casted protein sample to wash off excess salts.
- Dry the sample in 37 ˚C overnight by covering a lid to avoid any contamination from the dust particles.
- Observe the samples in AFM at non-contact mode for morphological evaluation.
- Analyze the images and determine the morphological parameters using the Gwyddion software [23].

*Hydrodynamic diameter by dynamic light scattering (DLS)*

Protein aggregation is preceded by protein-protein interactions, which leads to protein colloidal instability [24]. Therefore, comparing the hydrodynamic diameters of the native and heat-induced protein samples is supposed to provide insight into the aggregation propensity [25]. DLS provides the hydrodynamic diameter ($d_H$) using the relative frequency of intensity/volume/number of particles. DLS is performed with Litesizer 500 (Anton Paar, Graz, Austria) at room temperature, and the relative number frequency was used to estimate $d_H$ values. The following parameters are used as input to the instrument:

- Dilute the stock BSA solution to a concentration of 1 mg/ml using TBS buffer.
- Place the sample in a DLS-specific cuvette and set the measurement angle to 175˚ (backscattering) and 90˚ (side scattering) for measuring the fluctuation in light intensity being scattered by the sample particles.
- Set the number of runs to 20, with an initial equilibration time of 1 min.
- DLS measuring instrument and software employ the Stokes-Einstein equation to find out the $d_H$ value of the sample, *i.e.*,

$$d_H = \frac{K_B T}{3\pi\eta D} \tag{2}$$

where, $K_B$ = Boltzmann constant,
$T$ = absolute temperature in Kelvin,
$\eta$ = viscosity of the solution,
$D$ = average diffusion coefficient of the solution.

- Remove the native BSA sample and place the heat-induced BSA sample for measurement.
- Repeat all the experiments at least three times, keeping all parameters constant across the replicates.
- Plot a graph of $d_H$ value (in nm) along with the standard deviation for both native and heat-induced BSA.

## Method validation and discussion

*Thioflavin-T assay and intrinsic fluorescence*

Fig. 1(a) indicates the ThT fluorescence emission at 482 nm of the native and the heat-induced BSA samples after excitation at 450 nm. As it is known that BSA undergoes temperature-induced unfolding [15,26], it is quite probable for the native sample to form pre-fibrillar aggregates over heat induction. Since ThT is amyloid-specific, the increase in fluorescence of the heat-induced sample might indicate the unfolding and aggregation of BSA due to thermal incubation at 60 ˚C.

Intrinsic fluorescence spectroscopy, on the other hand, was performed by exciting the native and the heat-induced protein samples at 280 nm and recording the emission spectra at 300–450 nm. Fig. 1(b) indicates the emission maxima of the native BSA sample to be at around 332 nm, indicating the non-polar environment of the aromatic amino acid residues. In contrast, the heat-induced sample shows a fluorescence quenching behavior as compared to the native and also has a blue shift at 326 nm. Since blue shift confers a non-polar environment, this could mean a further packed protein structure. Such a packed structure could only arise due to heat-induced intermolecular interactions or aggregation.

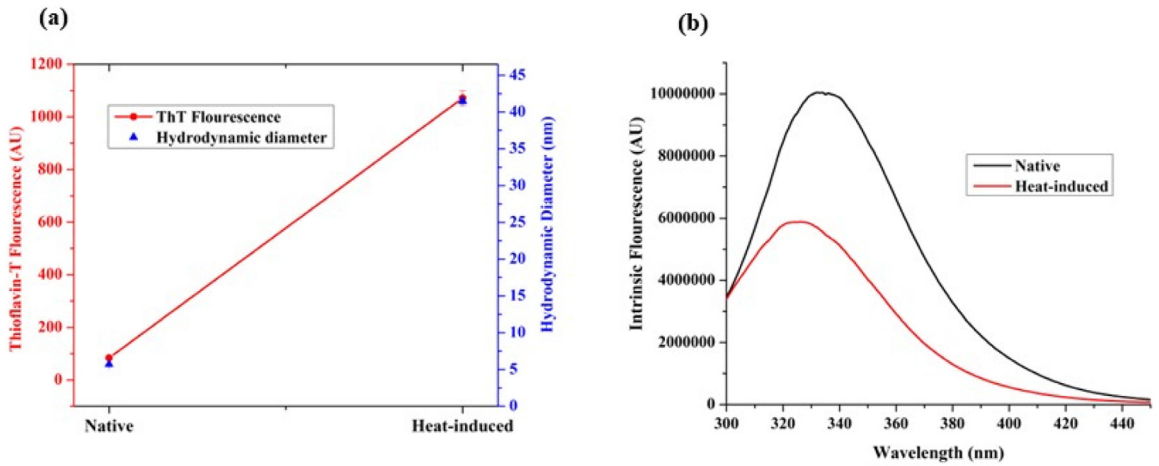


**Fig. 1.** (a) Thioflavin-T (ThT) binding fluorescence for the native and temperature-induced aggregated BSA. High fluorescence intensity for the heat-induced BSA is observed due to the stacking of ThT onto BSA amyloid fibrils formed because of overnight thermal incubation at 60 ˚C. Hydrodynamic diameter (nm) is also represented on the other Y-axis. The hydrodynamic diameter of the heat-induced BSA is found to be increased as compared to that of the native BSA. (b) The emission maximum of the native BSA is found to be at around 332 nm, whereas that for the heat-induced sample was found to be near 326 nm, indicating a blue shift.

*Circular dichroism*

FTIR and CD analyses are performed to determine the secondary structures of native BSA and subsequent changes after heat treatment. The far UV-CD spectra analysis is done in the wavelength range of 190–260 nm. The online webserver DichroWeb was used with the analysis method of CDSSTR, and reference set SMP180 (optimized for 180–240 nm) to convert machine unit ($\theta$) to MRE. As indicated in Fig. 2(a), the native spectrum represents a typical $\alpha$-helix pattern with a positive peak at 195 nm and two prominent negative dips at 208 and 222 nm. However, the heat-induced BSA protein sample indicates apparent changes at the mentioned usual wavelengths. A decrease in the MRE value is observed in the case of the positive peak at 195 nm, whereas an increased MRE value could be observed in the case of the negative dips at 208 and 222 nm. This could be an indication of decreased $\alpha$-helix pattern in the case of heat-induced aggregated BSA sample, with increased disorderedness. Fig. 2(b) depicts the percentage of secondary structural components observed in the CD spectra of both samples obtained from the DichroWeb server. The percentage of $\alpha$-helix decreased from 64 % in the native sample to 51 % in the heat-induced BSA sample, whereas the same for $\beta$-sheet increased from 8 % in native sample to 14 % in the heat-induced sample.

*FTIR spectroscopy*

The FTIR spectra of native and heat-treated BSA samples in the amide-I region are shown in Fig. 2(c). The peak in the range of 1640–1655 $cm^{-1}$ depicts the $\alpha$-helix and the random coil secondary structures. The range between 1615 and 1635 $cm^{-1}$ and 1695 $cm^{-1}$ corresponds to $\beta$-sheet, whereas that between 1665 and 1680 $cm^{-1}$ corresponds to $\beta$-turn [27]. Fig. 2(c) indicates a peak shift in the FTIR spectra of the native and heat-induced BSA solution, with the native spectrum having a sharp narrow peak at around 1651 $cm^{-1}$, corresponding to the $\alpha$-helical region. On the other hand, the spectrum of the heat-induced BSA protein shows peak broadening due to increased peak intersity in the $\beta$-sheet region. The native protein was observed to contain around 63 % of $\alpha$-helix, 25 % of $\beta$-sheet and 10 % of turn (Fig. 2d). This value is found to be similar to that calculated from the CD spectroscopic data of Fig. 2(b). However, in the heat-induced BSA solution, the percentage of $\alpha$-helix decreased to 58 %, whereas that of $\beta$-sheet increased to about 30 %. The increased percentage of $\beta$-sheet correlates well with the ThT fluorescence intensity, indicating the formation of $\beta$-sheet-rich aggregates.

*Atomic force microscopy and dynamic light scattering*

The morphology of the samples was analyzed using the AFM instrument. Fig. 3(a) indicates the AFM image of the native BSA solution. The native protein structure is almost observed to be spherical in structure, measuring about 25–40 nm as evaluated from the Gwyddion software. The dimension of the attached image is 1 x 1 μm. The temperature-induced aggregated sample contained different short fibrillar structures ranging from 51 to 119 nm (Fig. 3b).

With DLS measurements, the average $d_H$ value of the native BSA solution was found to be about 5 nm, whereas the heat-induced sample has a $d_H$ value of about 40 nm (Fig. 1a). The average polydispersity indices of the native and heat-induced BSA samples were observed to be 7.61 % and 17.64 %, respectively. The dimension measured from the AFM images is somewhat higher, presumably because of the overestimation of the size by a certain radius of the AFM tip, which is about 10 nm.

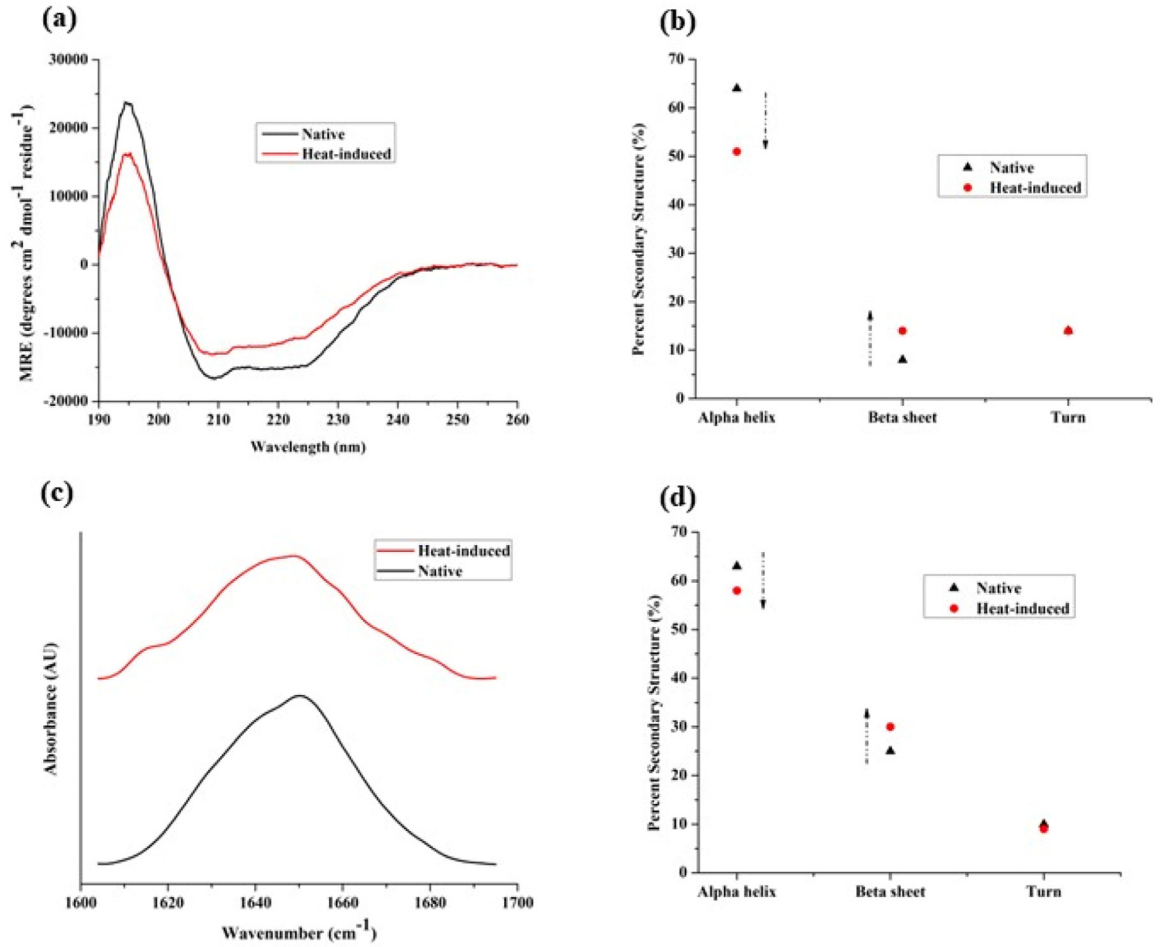


**Fig. 2.** (a). CD spectroscopic curve for the native and temperature-induced aggregated BSA. The native (dark-colored) sample depicts a positive peak at 195 nm and two prominent negative dips at 208 and 222 nm, which is a typical CD pattern of an $\alpha$-helix. However, altered peaks were observed for the heat-induced BSA (red-colored). (b). Percentage of $\alpha$-helix, $\beta$-sheets, $\beta$-turns, and unordered structures observed from the CD spectra of both samples obtained from the DichroWeb server. Respective increases and decreases are indicated with arrows. (c). The FTIR spectra in the amide-I region (1600–1700 cm$^{-1}$) of native and heat-treated BSA. Peak shift is observed in the FTIR spectrum of the native and heat-induced BSA solution. **(d).** Percentage of secondary structural components observed from the FTIR spectra of both the samples obtained after deconvolution. Respective increases and decreases are indicated with arrows.

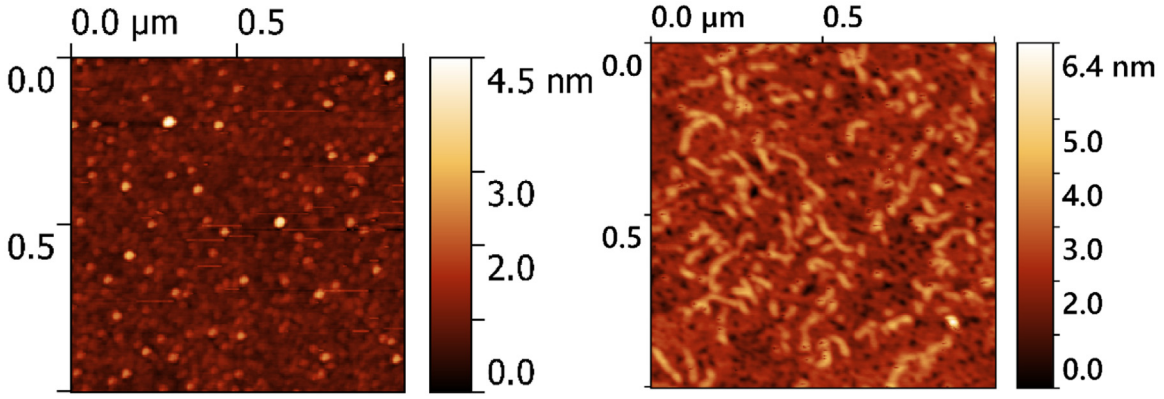


**Fig. 3.** AFM images of the (a) native and (b) heat-induced BSA samples.

## Conclusion

Multiple methods exist to detect changes in protein secondary structure over the course of heat-induced protein aggregation, and the present study effectively summarized some easily accessible methods. Structural differences between the native and the heat-induced BSA samples were determined using various analytical techniques. The aggregation propensity in terms of the increased $\beta$-sheets-rich fibrils with the heat-induced sample was determined through ThT fluorescence assay. The change in the microenvironment of the aromatic amino acids as a result of the thermal incubation was also determined from the intrinsic fluorescence of the protein. With the heat-induced sample, a blue shift from the native emission maxima at 332 nm to 326 nm indicated a more non-polar microenvironment. It could mean an increased intramolecular interaction, indicating the formation of higher-ordered intermediates.

The formation of $\beta$-sheets-rich fibrils in the heat-induced BSA sample was further verified by changes in the secondary structural analysis via CD and FTIR spectroscopy. From CD analysis, native BSA was observed to be of typical $\alpha$-helical structure with a positive peak at 195 nm and two prominent negative dips at 208 and 222 nm. The peak magnitudes were decreased in the case of the heat-induced sample. The FTIR and CD spectra indicated decrease in the contents of $\alpha$-helical structure and an increase in the percentage of $\beta$-sheet.

The hydrodynamic diameter of the heat-induced BSA sample was also observed to be around eight times that of the native protein. Finally, with the heat induction, native spherical morphology changes to short, prolonged structures of about 51–119 nm, indicating the formation of prefibrillar aggregates.

The analytical tools described here provide easy and robust methods which can be applied to laboratories without restrictions. With quick sample preparation and efficient measurement conditions, the mentioned methodologies fit into the research time frame for fast and efficient detection of protein fibrils. We expect this article to be helpful to the industry and academia in detecting protein fibrillation, thereby reducing these unwanted phenomena and improving therapeutic formulation stability and efficacy.

## Declaration of Competing Interest

The authors declare that they have no known competing financial interests or personal relationships that could have appeared to influence the work reported in this paper.

## Data availability

Data will be made available on request.

## References

[1] S. Alberti, A.A. Hyman, Biomolecular condensates at the nexus of cellular stress, protein aggregation disease and ageing, Nat. Rev. Mol. Cell Biol. 22 (2021) 196–213, doi:10.1038/s41580-020-00326-6.
[2] L.M. Pandey, Physicochemical factors of bioprocessing impact the stability of therapeutic proteins, Biotechnol. Adv. 55 (2022) 107909, doi:10.1016/j.biotechadv.2022.107909.
[3] M.L.E. Lundahl, S. Fogli, P.E. Colavita, E.M. Scanlan, Aggregation of protein therapeutics enhances their immunogenicity: causes and mitigation strategies, RSC Chem. Biol. 2 (2021) 1004–1020, doi:10.1039/D1CB00067E.
[4] C. Soto, S. Pritzkow, Protein misfolding, aggregation, and conformational strains in neurodegenerative diseases, Nat. Neurosci. 21 (2018) 1332–1340, doi:10.1038/s41593-018-0235-9.
[5] C. Panda, et al., Aggregated Tau-PHF6 (VQIVYK) potentiates NLRP3 inflammasome expression and autophagy in human microglial cells, Cells 10 (2021), doi:10.3390/cells10071652.
[6] C. Panda, S. Kumar, S. Gupta, L.M. Pandey, Structural, kinetic, and thermodynamic aspects of insulin aggregation, Phys. Chem. Chem. Phys. (2023), doi:10.1039/D3CP03103A.
[7] A. Singh, P. Datta, L.M. Pandey, Deciphering the mechanistic insight into the stoichiometric ratio dependent behavior of Cu(II) on BSA fibrillation, Int. J. Biol. Macromol. 97 (2017) 662–670, doi:10.1016/j.ijbiomac.2017.01.045.
[8] L.G. Sharma, L.M. Pandey, Shear-induced aggregation of amyloid $\beta$ (1–40) in a parallel plate geometry, J. Biomol. Struct. Dyn. 39 (2021) 6415–6423, doi:10.1080/07391102.2020.1798814.
[9] C. Xue, T.Y. Lin, D. Chang, Z. Guo, Thioflavin T as an amyloid dye: fibril quantification, optimal concentration and effect on aggregation, R. Soc. Open Sci. 4 (2017) 160696, doi:10.1098/rsos.160696.
[10] P. Sindrewicz, et al., Intrinsic tryptophan fluorescence spectroscopy reliably determines galectin-ligand interactions, Sci. Rep. 9 (2019) 11851, doi:10.1038/s41598-019-47658-8.
[11] M. Makarska-Bialokoz, Interactions of hemin with bovine serum albumin and human hemoglobin: a fluorescence quenching study, Spectrochim. Acta Part A 193 (2018) 23–32, doi:10.1016/j.saa.2017.11.063.
[12] ed N. Hellmann, D. Schneider, A.E. Kister, Protein Supersecondary Structures: Methods and Protocols Springer, New York, 2019. ed379-401.
[13] N.J. Greenfield, Using circular dichroism collected as a function of temperature to determine the thermodynamics of protein unfolding and binding interactions, Nat. Protoc. 1 (2006) 2527–2535, doi:10.1038/nprot.2006.204.
[14] M. Necci, et al., Critical assessment of protein intrinsic disorder prediction, Nat. Methods 18 (2021) 472–481, doi:10.1038/s41592-021-01117-3.
[15] L.G. Sharma, L.M. Pandey, Thermomechanical process induces unfolding and fibrillation of bovine serum albumin, Food Hydrocoll. 112 (2021) 106294, doi:10.1016/j.foodhyd.2020.106294.
[16] N. Mahanta, S. Sharma, L.G. Sharma, L.M. Pandey, U.S. Dixit, Unfolding of the SARS-CoV-2 spike protein through infrared and ultraviolet-C radiation based disinfection, Int. J. Biol. Macromol. 221 (2022) 71–82, doi:10.1016/j.ijbiomac.2022.08.197.
[17] A.J. Miles, S.G. Ramalli, B.A. Wallace, Dichroweb, a website for calculating protein secondary structure from circular dichroism spectroscopic data, Protein Sci. 31 (2022) 37–46, doi:10.1002/pro.4153.
[18] C. Louis-Jeune, M.A. Andrade-Navarro, C. Perez-Iratxeta, Prediction of protein secondary structure from circular dichroism using theoretically derived spectra, Proteins Struct. Funct. Bioinf. 80 (2012) 374–381, doi:10.1002/prot.23188.
[19] A. Micsonai, et al., BeStSel: webserver for secondary structure and fold prediction for protein CD spectroscopy, Nucleic Acids Res. 50 (2022) W90–W98, doi:10.1093/nar/gkac345.
[20] L. Comez, P.L. Gentili, M. Paolantoni, A. Paciaroni, P. Sassi, Heat-induced self-assembling of BSA at the isoelectric point, Int. J. Biol. Macromol. 177 (2021) 40–47, doi:10.1016/j.ijbiomac.2021.02.112.

[21] G. Baird, et al., FTIR spectroscopy detects intermolecular $\beta$-sheet formation above the high temperature tm for two monoclonal antibodies, Protein J. 39 (2020) 318–327, doi:10.1007/s10930-020-09907-y.
[22] F.S. Ruggeri, T. Šneideris, M. Vendruscolo, T.P.J. Knowles, Atomic force microscopy for single molecule characterisation of protein aggregation, Arch. Biochem. Biophys. 664 (2019) 134–148, doi:10.1016/j.abb.2019.02.001.
[23] P. Klapetek, D. Nečas, Independent analysis of mechanical data from atomic force microscopy, Meas. Sci. Technol. 25 (2014) 044009, doi:10.1088/0957-0233/25/4/044009.
[24] L. Nicoud, M. Lattuada, A. Yates, M. Morbidelli, Impact of aggregate formation on the viscosity of protein solutions, Soft Matter 11 (2015) 5513–5522, doi:10.1039/C5SM00513B.
[25] S. Brudar, B. Hribar-Lee, Effect of buffer on protein stability in aqueous solutions: a simple protein aggregation model, J. Phys. Chem. B 125 (2021) 2504–2512, doi:10.1021/acs.jpcb.0c10339.
[26] V.A. Borzova, et al., Kinetics of thermal denaturation and aggregation of bovine serum albumin, PLoS One 11 (2016) e0153495, doi:10.1371/journal.pone.0153495.
[27] A. Hasan, G. Waibhaw, L.M. Pandey, Conformational and organizational insights into serum proteins during competitive adsorption on self-assembled monolayers, Langmuir 34 (2018) 8178–8194, doi:10.1021/acs.langmuir.8b01110.